Rcan1 negatively regulates FcεRI-mediated signaling and mast cell function

Yong Jun Yang,[1] Wei Chen,[1] Alexander Edgar,[1] Bo Li,[2] Jeffery D. Molkentin,[3] Jason N. Berman,[1] and Tong-Jun Lin[1]

[1]Department of Microbiology and Immunology and Department of Pediatrics, Dalhousie University, Halifax, Nova Scotia B3K 6R8, Canada
[2]Department of Immunology, Capital Medical University, Beijing 100069, China
[3]Department of Pediatrics, Cincinnati Children's Hospital Medical Center, University of Cincinnati, Cincinnati, OH 45229

Aggregation of the high affinity IgE receptor (FcεRI) activates a cascade of signaling events leading to mast cell activation. Subsequently, inhibitory signals are engaged for turning off activating signals. We identified that regulator of calcineurin (Rcan) 1 serves as a negative regulator for turning off FcεRI-mediated mast cell activation. FcεRI-induced Rcan1 expression was identified by suppression subtractive hybridization and verified by real-time quantitative polymerase chain reaction and Western blotting. Deficiency of *Rcan1* led to increased calcineurin activity, increased nuclear factor of activated T cells and nuclear factor κB activation, increased cytokine production, and enhanced immunoglobulin E–mediated late-phase cutaneous reactions. Forced expression of Rcan1 in wild-type or *Rcan1*-deficient mast cells reduced FcεRI-mediated cytokine production. *Rcan1* deficiency also led to increased FcεRI-mediated mast cell degranulation and enhanced passive cutaneous anaphylaxis. Analysis of the *Rcan1* promoter identified a functional Egr1 binding site. Biochemical and genetic evidence suggested that Egr1 controls Rcan1 expression. Our results identified Rcan1 as a novel inhibitory signal in FcεRI-induced mast cell activation and established a new link of Egr1 and Rcan1 in FcεRI signaling.

CORRESPONDENCE
Tong-Jun Lin:
tong-jun.lin@dal.ca

Abbreviations used: BMMC, bone marrow–derived mast cell; ChIP, chromatin immunoprecipitation; DNFB, dinitrofluorobenzene; JNK, c-Jun N-terminal kinase; MAPK, mitogen-activated protein kinase; PI3K, phosphatidylinositol 3 kinase; Rcan, regulator of calcineurin; SSH, suppression subtractive hybridization.

Mast cells play a central role in IgE-dependent allergic diseases. Recently, mast cells have also been recognized as prominent immune effector cells. Mast cells constitutively express the high affinity IgE receptor (FcεRI) on their surface (1). Aggregation of FcεRI initiates a cascade of activating signaling events leading to the production of mast cell mediators. Activation signals are needed for the production and secretion of proinflammatory mediators. Activation signals are subsequently inhibited by negative signals that are required for mast cells to return to their basal resting condition (2). Thus, FcεRI-mediated activation and subsequent inhibition are highly ordered, sequential molecular events. The nature of this negative signaling event after FcεRI-mediated mast cell activation is the subject of this study.

FcεRI consists of an IgE-binding α subunit, a signal-amplifying β subunit, and two signal-initiating γ subunits (3). FcεRI-mediated activation events have been extensively studied. The widely accepted model is as follows: upon cross-linking of the FcεRI, the Src family protein tyrosine kinases Lyn and Fyn are activated (3–5). Lyn phosphorylates tyrosine residues of the immunoreceptor tyrosine-based activation motif in the β and γ subunits (3, 4). Syk is then recruited to the γ subunit and activates a multitude of protein kinases. Fyn functions to phosphorylate Gab2, which is involved in FcεRI-induced activation of phosphatidylinositol 3 kinase (PI3K) (5). Concerted actions of Lyn and Fyn activate several signaling pathways, including IκB–NF-κB, NFAT, mitogen-activated protein kinases (MAPKs), and PI3K–Akt, leading to mast cell degranulation and production of inflammatory cytokines and lipid mediators (1, 3). Most of these signal events are enzymatic reactions and occur within seconds to minutes.

In addition to the immediate enzymatic activation of protein kinases, we recently demonstrated that *Egr1*-deficient mast cells showed impaired FcεRI-induced TNF and IL-13

The Rockefeller University Press $30.00
J. Exp. Med. Vol. 206 No. 1 195-207
www.jem.org/cgi/doi/10.1084/jem.20081140

production (6). The de novo synthesis of the transcription factor Egr1 is required for the full responsiveness of mast cells in the production of cytokines in response to IgE stimulation (6). The promoter region of inflammatory cytokines such as TNF contains multiple transcription factor binding sites, including those for NF-κB, NFAT, and Egr1 (7, 8). Accordingly, the coordinated action of immediate enzymatic activation together with newly synthesized transcription factor Egr1 contributes to the magnitude of mast cell activation. As FcεRI aggregation–induced Egr1 expression occurs from 15 min to 1 h after antigen stimulation, it appears that Egr1 contributes to the later phase of FcεRI-mediated signals (6). Intriguingly, an opposing biological effect of Egr1, both the stimulatory and inhibitory effects on gene expression, has been reported (9–11). Such dual effects suggest that Egr1 may initiate both activation and inhibition signals.

Transcription factors NFAT and NF-κB regulate the transcription of multiple cytokines in mast cells. These transcription factors are sequestered in the cytoplasm under resting conditions and translocate to the nucleus upon FcεRI activation (12, 13). Calcineurin is capable of regulating NFAT and NF-κB nuclear translocation (14, 15). Blocking the calcineurin–NFAT pathway by using pharmaceutical molecules has been shown to be an effective means for treating allergic inflammation, highlighting the importance of this pathway in allergy (16).

A new family of regulators of calcineurin (Rcans), including Rcan1, Rcan2, and Rcan3, has been shown to modulate calcineurin activity under physiological and pathological conditions (17). In this study, we identified Rcan1 as an endogenous negative regulator in FcεRI-mediated signaling. *Rcan1* deficiency had few effects on the early phase (5–20 min) of FcεRI-induced NFAT and IκB activation but strongly enhanced the late-phase FcεRI-mediated NFAT activation (3–6 h) and IκB phosphorylation (1 h), leading to increased cytokine production in vitro and enhanced late-phase cutaneous allergic reaction in vivo. *Rcan1* deficiency also showed increased FcεRI-mediated mast cell degranulation in vitro and increased passive cutaneous anaphylaxis in vivo. Accordingly, Rcan1 is a novel negative regulator in FcεRI-induced mast cell activation. In addition, biochemical and genetic analyses revealed a new link between Egr1 and Rcan1 in FcεRI-mediated signaling.

RESULTS

FcεRI aggregation induces Rcan1 expression

Suppression subtractive hybridization (SSH) allows us to identify target genes even without a prerequisite knowledge of these genes. SSH was used to identify genes that are differentially expressed in FcεRI-activated mast cells. Total RNA from TNP-BSA–treated or untreated mouse bone marrow–derived mast cells (BMMCs) were used to generate double-stranded cDNAs. A subtracted cDNA library was constructed to enrich the transcripts that were differentially expressed by mast cells after TNP-BSA stimulation. The subtraction efficiency was evaluated by comparing GAPDH cDNA levels by PCR in serial dilutions of subtracted and nonsubtracted control cDNA (Fig. S1, available at http://www.jem.org/cgi/content/full/jem.20081140/DC1). The PCR products of the subtraction were cloned and sequenced after a differential hybridization procedure to exclude false positives. Surprisingly, among 33 positive clones sequenced, 8 clones matched the *Rcan1* gene (exons 4, 5, 6, and 7), suggesting the abundance of this gene product in FcεRI-activated mast cells (Table S1 and Fig. S2). One clone matched the *Egr1* gene (Table S1). Reverse Northern blot analysis using one of the identified Rcan1 clones (2C3) as a probe confirmed the increased expression of Rcan1 in the TNP-BSA–stimulated sample (Fig. 1 A).

We further examined the kinetics of Rcan1 expression in mast cells in response to FcεRI aggregation using real-time quantitative PCR. Given that the expression of any *Rcan* family members by mast cells has not been reported previously, we also examined Rcan2 and Rcan3. Two Rcan1 isoforms have been reported, the isoform Rcan1-4 encoded by exons 4, 5, 6, and 7, and the isoform Rcan1-1 encoded by exons 1, 5, 6, and 7 (17). Total RNA was isolated from TNP-BSA–treated mouse BMMCs and analyzed by real-time quantitative PCR for two Rcan1 isoforms, as well as for Rcan2 and Rcan3. Levels of Rcan mRNA expression were normalized to GAPDH in each sample. Rcan1-1 and Rcan3 showed low levels of expression under resting conditions, whereas Rcan2 was undetectable in both resting and activated cells (unpublished data). Among these Rcan family members tested, Rcan1-4 was the only member found to be up-regulated by TNP-BSA stimulation. The Rcan1-4 level in the unstimulated mast cells was undetectable. Rcan1-4 expression peaked at 60 min after TNP-BSA stimulation (Fig. 1 B). PCR-amplified *Rcan1* products (Rcan1-4) were also separated in agarose gels and visualized by ethidium bromide staining. A representative gel is presented in Fig. 1 C. Strong Rcan1-4 expression can be seen at 60 min after TNP-BSA stimulation.

To determine Rcan1 expression at the protein level, IgE-sensitized mast cells were treated with TNP-BSA for various times and subjected to Western blot analysis. Rcan1 expression was observed in TNP-stimulated mast cells (Fig. 1 D).

Development of mast cells in the absence of Rcan1

To examine a role of Rcan1 in IgE-dependent mast cell activation, we chose to obtain mouse BMMCs from *Rcan1*-deficient mice. Exons 5 and 6 are deleted from the *Rcan1* gene. Thus, these mice are deficient in *Rcan1* products (Rcan1-1 and Rcan1-4) (18). Bone marrow cells from *Rcan1*-deficient and wild-type mice were cultured in conditioned medium and were analyzed by flow cytometry for c-kit and IgE receptor expression. No difference of the c-kit and IgE receptor expression after 5 wk of culture was observed between wild-type and *Rcan1*-deficient cells (Fig. S3 A, available at http://www.jem.org/cgi/content/full/jem.20081140/DC1). BMMCs were also used for Toluidine blue staining. Morphologically, no difference was observed between *Rcan1*-deficient and wild-type mast cells (Fig. S3 B). This result suggests that mast cells mature normally in the absence of Rcan1.

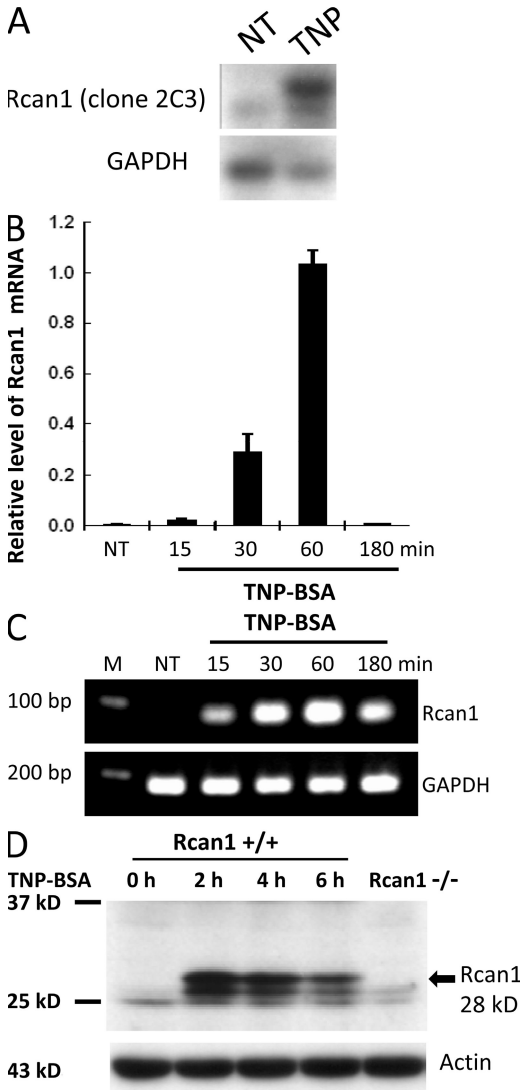

Figure 1. IgE-dependent Rcan1 expression by mast cells. (A) RNAs from TNP-BSA–treated (TNP) and untreated (NT) mouse BMMCs were reversed transcribed into cDNA and blotted with a GAPGH probe or a Rcan1 probe obtained from clone 2C3 in the SSH assay. A representative Northern blot from two independent experiments is shown. (B and C) BMMCs were sensitized with anti-TNP IgE and stimulated with 10 ng/ml TNP-BSA for 15, 30, 60, or 180 min. RNA isolated from these cells was reverse transcribed to cDNA and subjected to real-time quantitative PCR. Rcan1 expression was normalized to endogenous control GAPDH. The data are expressed as relative mRNA levels compared with the mean expression level in BMMCs treated with TNP-BSA for 60 min (=1), because at this time point Rcan1 showed the highest expression level. The PCR products were also separated by agarose gel and stained with ethidium bromide. Untreated BMMCs (NT) showed no Rcan1 expression, whereas TNP induced a strong Rcan1 expression. Error bars represent SEs from three independent experiments. (D) IgE-sensitized BMMCs were treated with TNP-BSA for 2, 4, or 6 h. Cell lysates were analyzed by Western blotting for Rcan1. TNP-induced Rcan1 expression was observed in wild-type BMMCs ($Rcan1^{+/+}$). Lysate from Rcan1-deficient BMMCs ($Rcan1^{-/-}$) after TNP treatment (2 h) was used as a control. Membrane was stripped and probed for actin as a loading control. A representative Western blot from two independent experiments is shown.

Increased activation of NFAT and NF-κB pathways but not MAPKs in *Rcan1*-deficient BMMCs

To determine the specific signaling pathways regulated by Rcan1 in FcεRI-mediated mast cell activation, we examined activation of NFAT, NF-κB, and MAPK pathways in *Rcan1*-deficient BMMCs. For the study of NFAT pathway activation, an NFAT luciferase assay, EMSA, and an immunofluorescence assay were used. *Rcan1*-deficient and wild-type BMMCs were transfected with NFAT luciferase plasmid. Cells were then sensitized with anti-TNP IgE and activated with TNP-BSA for 18 h. A significant increase in NFAT luciferase activity was seen in *Rcan1*-deficient BMMCs after TNP-BSA stimulation compared with that in wild-type BMMCs (Fig. 2 A). These data suggests that Rcan1 is a negative regulator of IgE-dependent NFAT activation.

To further examine NFAT activation, an NFAT DNA probe was synthesized based on the NFAT binding sequence in the mouse *IL-13* promoter and labeled with ^{32}P. Nuclear extracts from *Rcan1*-deficient and wild-type BMMCs after TNP stimulation for various times (5–360 min) were subjected to EMSA using a ^{32}P-labeled NFAT probe. As shown in Fig. 2 B, NFAT activities were enhanced in *Rcan1*-deficient BMMCs at the later time points (180 and 360 min) after TNP stimulation. In contrast, little difference was observed at the early time points (5–60 min) between *Rcan1*-deficient and wild-type BMMCs. This result suggests that Rcan1 is a negative regulator by turning off the TNP-activated NFAT signal. Densitometry analysis of NFAT DNA binding activity is shown in Fig. 2 C. The binding specificity of nuclear proteins to the NFAT DNA sequence was verified through competitive binding by the nonradioisotope-labeled NFAT probe but not by a mutant probe (Fig. 2 D). The binding specificity was further verified by supershift assay. Nuclear protein binding to the NFAT probe was strongly blocked by anti-NFATc1 antibody or by anti-NFATc2 antibody (Fig. 2 E).

To examine whether Rcan1 regulates calcineurin activity in mast cells, *Rcan1*-deficient and wild-type BMMCs were sensitized with IgE and treated with TNP-BSA. BMMCs were then lysed and subjected to analysis for calcineurin activity. Increased calcineurin activity was observed in *Rcan1*-deficient BMMCs (Fig. 2 F).

To examine NFAT nuclear translocation, IgE-sensitized BMMCs were treated with TNP-BSA for 6 h. Cells were then fixed, permeabilized, and stained with anti-NFATc1 antibody. The cell nucleus was visualized by DAPI staining. TNP-induced NFAT nuclear translocation was visible in wild-type and *Rcan1*-deficient cells. Enhanced NFAT nuclear translocation was seen in *Rcan1*-deficient cells when compared with wild-type cells (Fig. S4, available at http://www.jem.org/cgi/content/full/jem.20081140/DC1).

In light of a critical role for transcription factor NF-κB in the regulation of gene expression (19), we examined whether Rcan1 is required in FcεRI-mediated NF-κB pathway activation. *Rcan1*-deficient BMMCs and wild-type cells were transfected with NF-κB luciferase plasmid. After sensitization with anti-TNP IgE, BMMCs were stimulated with TNP-BSA for 5 h.

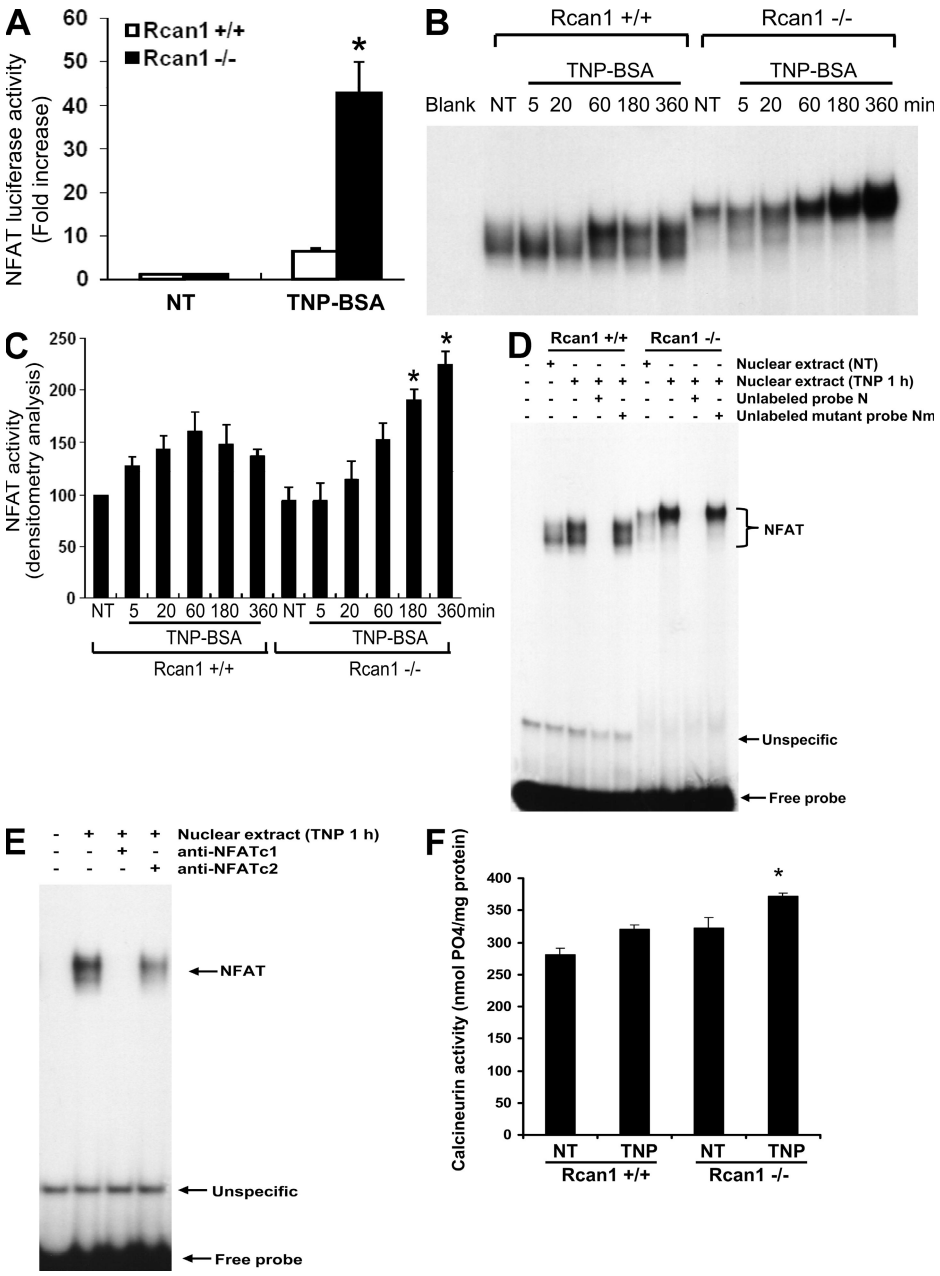

Figure 2. ***Rcan1*** **deficiency leads to increased IgE-dependent NFAT activation.** (A) Rcan1$^{+/+}$ and Rcan1$^{-/-}$ BMMCs were transfected with a pNFAT-Luc and the control reporter plasmid pRL-TK. After transfection (24 h), cells were sensitized with anti-TNP IgE for 18 h. Then cells were either left untreated (NT) or treated with 10 ng/ml TNP-BSA for 18 h (TNP). Firefly and Renilla activities were sequentially quantified using a dual-luciferase reporter assay system. Data are means ± SEM (n = 3 independent experiments). *, P < 0.05 compared with wild-type group. (B) NFAT binding concensus sequence (N) on mouse IL-13 promoter 5′-AAGGTGTTTCCCCAAGCCTTTCCC-3′ was labeled with ^{32}P for EMSA. After sensitization with anti-TNP IgE, Rcan1$^{+/+}$ and Rcan1$^{-/-}$ BMMCs were either not treated (NT) or stimulated with 10 ng/ml TNP-BSA for 5, 20, 60, 180, and 360 min. Nuclear proteins were isolated and subjected to EMSA. Shown is a representative from six independent experiments. (C) Densitometry analysis of NFAT activation by EMSA was performed based on six experiments. *, P < 0.05 compared with the same time point of the wild-type group (180 or 360 min). (D) Nuclear extracts from Rcan1$^{+/+}$ and Rcan1$^{-/-}$ BMMCs were used for competition assays. 50× concentrated unlabeled NFAT probe (N) was used to compete with the ^{32}P-labeled NFAT probe, whereas 50× concentrated unlabeled mutant NFAT probe (Nm; 5′-AAGGTGT*CCAT*CCAAGCCT*CCTA*C-3′) was used as a control. 1 µl of nonradiolabeled wild-type NFAT probe (N) or mutant probe Nm were added and incubated for 15 min before the addition of the radiolabeled probe. (E) Antibody blockade of the DNA–protein complex formation (supershift assay). Nuclear proteins from BMMCs treated for 1 h with 10 ng/ml TNP-BSA were incubated with or without specific antibodies to NFATc1 or NFATc2 for 30 min on ice before EMSA experiments using the ^{32}P-labeled NFAT probe (N). Shown is a representative from three (D) or two (E) independent experiments. (F) Rcan1$^{+/+}$ and Rcan1$^{-/-}$ BMMCs were treated with 10 ng/ml TNP-BSA for 6 h or left untreated. Cells were lysed, and calcineurin activity was analyzed by using a calcineurin assay kit according to the manufacturer's instructions. Error bars represent SE (n = 4). *, P < 0.05 compared with the TNP-treated Rcan1$^{+/+}$ group.

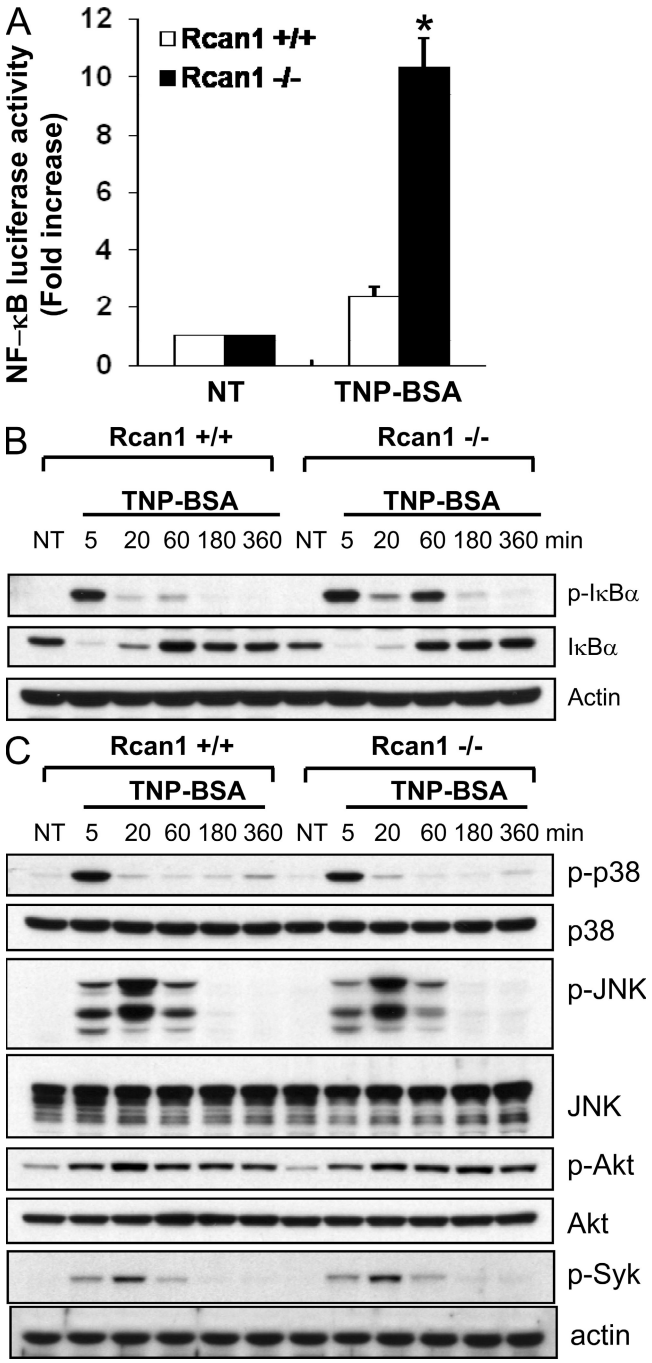

Figure 3. *Rcan1* deficiency induces increased IgE-dependent NF-κB activation but not MAPK, Akt, or Syk. (A) Rcan1$^{+/+}$ and Rcan1$^{-/-}$ BMMCs were transfected with a pNF-κB-Luc and the control reporter plasmid pRL-TK. After transfection (24 h), cells were sensitized with anti-TNP IgE for 5 h. Cells were then either left untreated (NT) or treated with 10 ng/ml TNP-BSA for 18 h (TNP). Firefly and Renilla activities were sequentially quantified using a dual-luciferase reporter assay system. Data are means ± SEM (n = 3 independent experiments). *, $P < 0.05$ compared with the wild-type group. (B and C) Rcan1$^{+/+}$ and Rcan1$^{-/-}$ BMMCs were sensitized with anti-TNP IgE and stimulated with TNP-BSA for various times. Total cell lysates were analyzed by Western blotting for various phosphorylated and total proteins. Increased IκB phosphorylation in Rcan1$^{-/-}$ BMMCs was found at 60 min after TNP stimulation when compared with Rcan1$^{+/+}$ cells. In contrast, the pattern of TNP-induced phosphorylation of p38, JNK, Akt, and Syk is similar between Rcan1$^{-/-}$ and Rcan1$^{+/+}$ BMMCs.

As shown in Fig. 3 A, *Rcan1*-deficient BMMCs showed significantly enhanced NF-κB activity in response to TNP stimulation, suggesting that Rcan1 is needed for the negative regulation of FcεRI-mediated NF-κB activation. NF-κB activity is regulated by IκB. The effects of Rcan1 on FcεRI-mediated IκB phosphorylation and degradation were examined by Western blotting. Aggregation of FcεRI induced a rapid phosphorylation of IκB (5 min), followed by IκB degradation (5 and 20 min) and subsequent regeneration of this molecule (60, 180, and 360 min; Fig. 3 B). Interestingly, the early events of IκB phosphorylation and degradation at 5 and 20 min were not affected by *Rcan1* deficiency. In contrast, phosphorylation at the later time point (60 min) was significantly enhanced in *Rcan1*-deficient BMMCs (Fig. 3 B). This process was associated with an increased regeneration of IκBα at 60 min after TNP-BSA stimulation (Fig. S5, available at http://www.jem.org/cgi/content/full/jem.20081140/DC1). These results suggest that Rcan1 is likely involved in "turning off" FcεRI-mediated activation signals, a notion consistent with that in NFAT signaling.

MAPKs represent a distinct mechanism in the regulation of mast cell function. Previous studies have established a major role of the MAPKs c-Jun N-terminal kinase (JNK) and p38 in FcεRI-mediated mast cell activation (20, 21). Accordingly, we tested whether Rcan1 affects FcεRI-mediated JNK and p38 signaling. Cell lysates from TNP-stimulated BMMCs were subjected to Western blotting for phospho-JNK, phospho-p38, and their total proteins. As shown in Fig. 3 C, TNP stimulation induced an increase of p38 phosphorylation (5 min) and JNK phosphorylation (20 min). Subsequently, levels of p38 and JNK phosphorylation returned to basal conditions (180–360 min). Similar patterns of TNP-induced phosphorylation (the increase in the early phase and decrease in the late phase) of p38 and JNK were observed for *Rcan1*-deficient and wild-type mast cells. These data suggest that Rcan1 is not required for FcεRI-mediated MAPK activation and inactivation processes. We also tested Akt phosphorylation, which is involved in the activation of the PI3K pathway. Similarly, no difference in the Akt phosphorylation pattern was observed between *Rcan1*-deficient and wild-type BMMCs (Fig. 3 C). In addition, a similar pattern of FcεRI-mediated Syk phosphorylation was observed between wild-type and *Rcan1*-deficient BMMCs (Fig. 3 C).

Rcan1 deficiency leads to enhanced IL-6, IL-13, and TNF production in response to TNP stimulation

Several cytokines such as IL-6, IL-13, and TNF play important roles in allergy and are regulated by the transcription factors NFAT and NF-κB. To determine whether Rcan1 is involved in the regulation of FcεRI-mediated cytokine

production, *Rcan1*-deficient and wild-type BMMCs were sensitized with anti-TNP IgE and stimulated with TNP-BSA for various times. IL-6, IL-13, and TNF production in cell-free supernatants was determined by ELISA. Expression of these cytokine mRNAs was analyzed by real-time quantitative PCR using total RNA isolated from cell pellets. Production of IL-6 was significantly enhanced by 87, 170, and 115% at the time points of 3, 6, and 18 h, respectively, in *Rcan1*-deficient BMMCs compared with wild-type BMMCs (Fig. 4 A). Importantly, real-time PCR analysis revealed that TNP-BSA–induced IL-6 mRNA expression was prolonged in *Rcan1*-deficient BMMCs (Fig. 4 B). PCR-amplified products separated by agarose gel electropheresis also revealed a prolonged TNP-BSA–induced IL-6 expression in *Rcan1*-deficient BMMCs (Fig. 4 C). Similarly, TNP-BSA–induced IL-13 and TNF production was enhanced at the protein level, whereas the mRNA expression of these cytokines was prolonged in *Rcan1*-deficient cells (Fig. 4, D–I). Enhanced production of IL-6, IL-13, and TNF at the protein level is likely caused by the prolonged mRNA expression of these cytokines. The prolonged mRNA expression of these cytokines supports the notion that Rcan1 functions as a negative regulator by turning off FcεRI-activated signals. This is consistent with the negative role of Rcan1 in the regulation of FcεRI-induced NFAT and IκB–NF-κB activation.

To further determine a role of Rcan1 in FcεRI-mediated cytokine production, wild-type and *Rcan1*-deficient BMMCs were transfected with Rcan1-pCMV vector or empty vector pCMV. These cells were then sensitized with anti-TNP IgE and stimulated with TNP-BSA. Cell supernatants were collected for testing cytokine production. Both wild-type and *Rcan1*-deficient cells transfected with Rcan1-pCMV showed

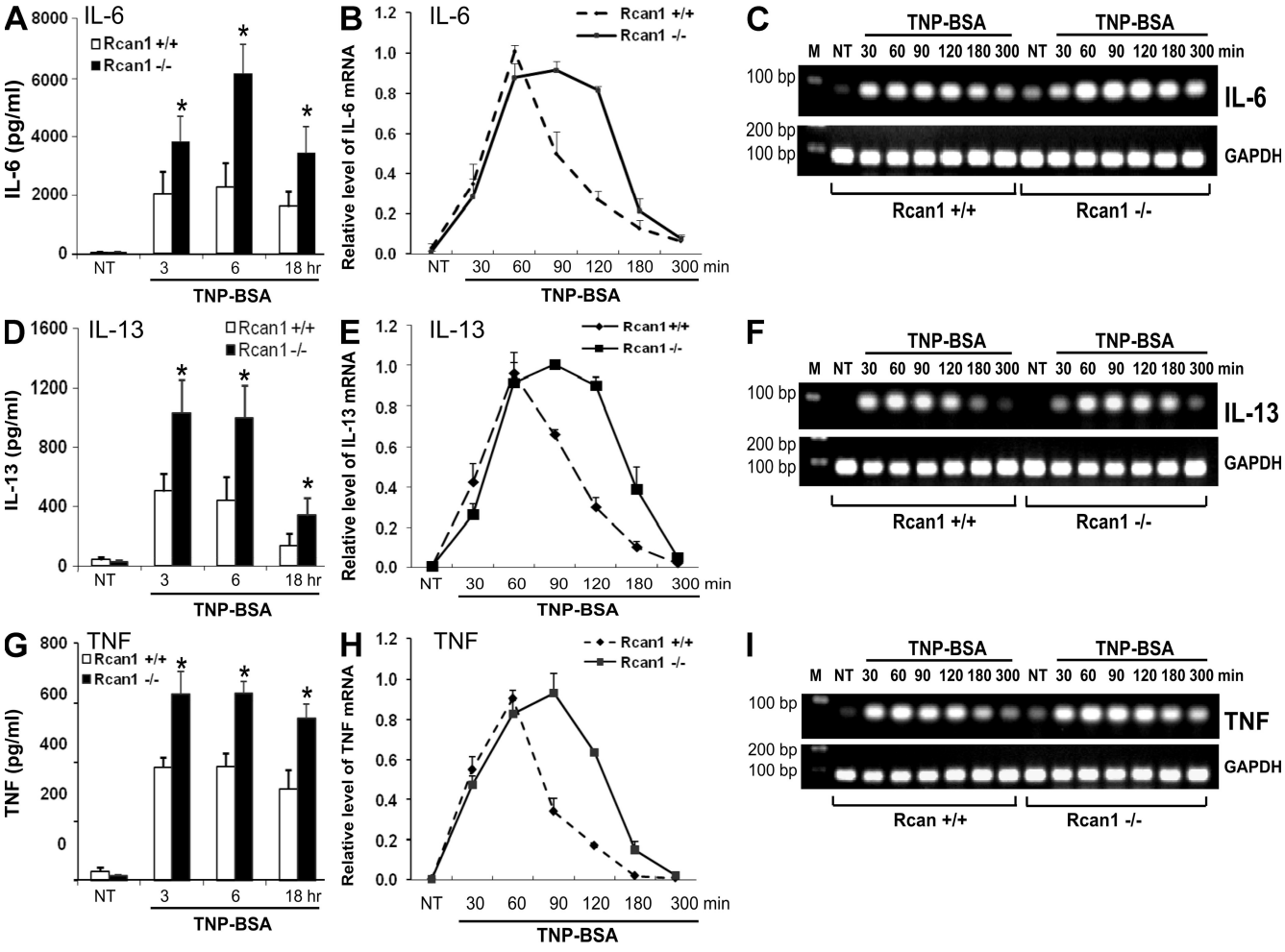

Figure 4. ***Rcan1*** **deficiency leads to enhanced IgE-dependent production of IL-6, IL-13, and TNF.** After sensitization with anti-TNP IgE for 24 h, Rcan1$^{+/+}$ and Rcan1$^{-/-}$ BMMCs were either not treated (NT) or stimulated with TNP-BSA for various times. Cell-free supernatants were collected for the detection of IL-6 (A), IL-13 (D), and TNF (G) by ELISA. Cell pellets were used for RNA isolation and analysis for cytokine mRNA expression. Real-time quantitative PCR was performed to determine IL-6 (B), IL-13 (E), and TNF (H) expression. IL-6, IL-13, and TNF expression was normalized to endogenous control GAPDH. The PCR products for IL-6 (C), IL-13 (F), and TNF (I) were also separated by agarose gel and stained with ethidium bromide. Untreated BMMCs (NT) showed little cytokine expression, whereas TNP induced enhanced cytokine production in Rcan1$^{-/-}$ BMMCs. Error bars represent SEs from six independent experiments (A, B, D, E, G, and H). Results presented in C, F, and I are representative of three to six separate experiments. *, $P < 0.05$ compared with the wild-type group.

decreased IL-6 and TNF production after TNP-BSA stimulation, suggesting that forced expression of Rcan1 reduced FcεRI-mediated cytokine production (Fig. 5).

Rcan1 deficiency leads to enhanced FcεRI-mediated late-phase cutaneous reaction in vivo

Mast cell–derived cytokines contribute to the development of late-phase allergic reactions (22, 23). To examine whether Rcan1 contributes to FcεRI-mediated late-phase cutaneous reaction in vivo, mice were sensitized with anti-DNP IgE 24 h before a solution of 0.3% dinitrofluorobenzene (DNFB; hapten) was applied epicutaneously to the ear skin or footpad. IgE/antigen-specific edema was determined by tissue weight and thickness. *Rcan1*-deficient mice exhibited increased IgE/antigen-specific edema when measured by tissue weight (Fig. 6, A and B). Tissue thickness, measured by a digital micrometer, also showed similar results (Fig. 6, C and D). These findings are consistent with the increased IL-6, IL-13, and TNF production by *Rcan1*-deficient BMMCs in vitro.

Rcan1 deficiency leads to enhanced FcεRI-mediated mast cell degranulation and passive cutaneous anaphylaxis in vivo

To examine whether Rcan1 plays a role in IgE-dependent mast cell degranulation, wild-type and *Rcan1*-deficient BMMCs were sensitized with anti-TNP IgE and stimulated with TNP-BSA for 20 min. Mast cell degranulation was determined by testing β-hexosaminidase release. Increased mast cell degranulation was observed in *Rcan1*-deficient mast cells (Fig. 6 E). Mast cell mediators released by degranulation contribute to the anaphylactic reactions in vivo. To examine whether *Rcan1* deficiency affects passive cutaneous anaphylaxis in vivo, the left ears of mice were passively sensitized with 20 ng anti-DNP IgE, whereas the right ears were injected with saline as a control. 24 h later, mice were injected with 100 μg DNP-BSA containing Evans blue dye via the tail vein. 30 min later, tissues from both ears were collected for extraction of Evans blue dye to determine vascular permeability. Increased vascular permeability (passive cutaneous anaphylaxis) was observed in *Rcan1*-deficient mice (Fig. 6 F).

To exclude the possibility that the increased cutaneous allergic responses is caused by the abnormal mast cell development in vivo, the ears, tongues, and back skin from *Rcan1*-deficient and wild-type mice were used to examine the presence of mast cells. A similar number and morphology of mast cells were observed in tissues from *Rcan1*-deficient and wild-type mice (Fig. 6, G and H).

FcεRI-induced Egr1 expression precedes Rcan1 expression

Next, we examined how the negative Rcan1 signal is activated during FcεRI activation. Our SSH assay using RNAs from TNP-BSA–stimulated BMMCs identified one clone (2A10) that matched the *Egr1* gene (Table S1). Real-time quantitative PCR analysis showed that *Egr1* gene expression peaked at 15 min after TNP-BSA stimulation. In contrast, Rcan1 expression began to increase at 15 min and peaked at 60 min (Fig. 7 A). These data suggested a sequential gene expression relationship between Egr1 and Rcan1 in mast cells and prompted us to analyze the promoter sequence of *Rcan1*, where we identified a putative Egr1 binding domain (Fig. 7 B).

Rcan1 promoter contains Egr1 binding activity

To determine whether the putative Egr1 binding sequence on the *Rcan1* promoter between −158 and −142 is functional, we generated a series of constructs for a luciferase assay containing various regions of the *Rcan1* promoter. All constructs start at −67 bp from the ATG codon. The 5′ end of each construct varies to include different parts of the putative Egr1 binding sequence (Fig. 7 C, left). Mouse BMMCs were transfected with these constructs, sensitized with anti-TNP IgE, and stimulated with TNP-BSA. Luciferase activity was determined. As shown in Fig. 7 C, both constructs pR-luc283 and pR-luc158, which contain the full length of the Egr1 binding sequence from −158 to −142, showed strong luciferase activity. The construct pR-luc154, which contains a partial Egr1 binding sequence from −154 to −142, showed

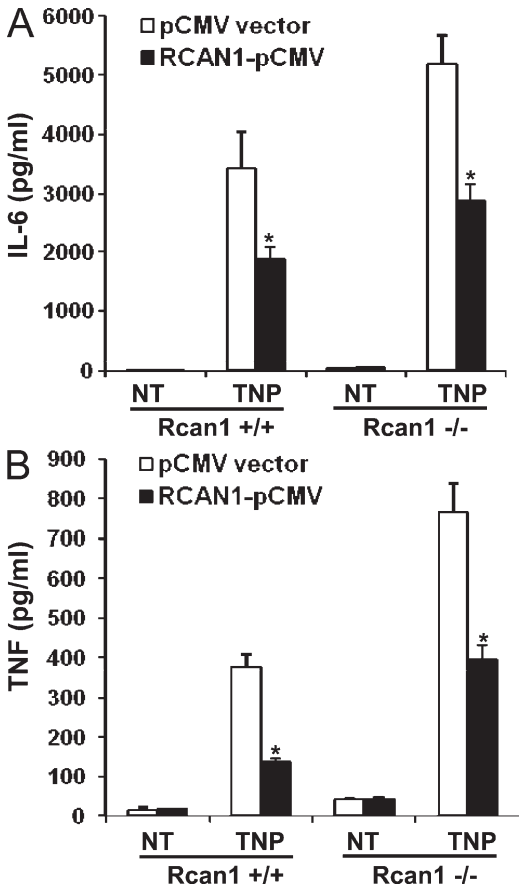

Figure 5. Forced Rcan1 expression reduced IgE-dependent cytokine production. Wild-type and *Rcan1*-deficient BMMCs were transfected with Rcan1-pCMV vector or control vector pCMV. These cells were then sensitized with anti-TNP IgE and subsequently stimulated with 10 ng/ml TNP-BSA for 6 h (TNP) or left untreated (NT). Cell-free supernatants were collected for the determination of IL-6 and TNF by ELISA. Error bars represent SE ($n = 3$). *, $P < 0.05$ compared with the control pCMV vector group.

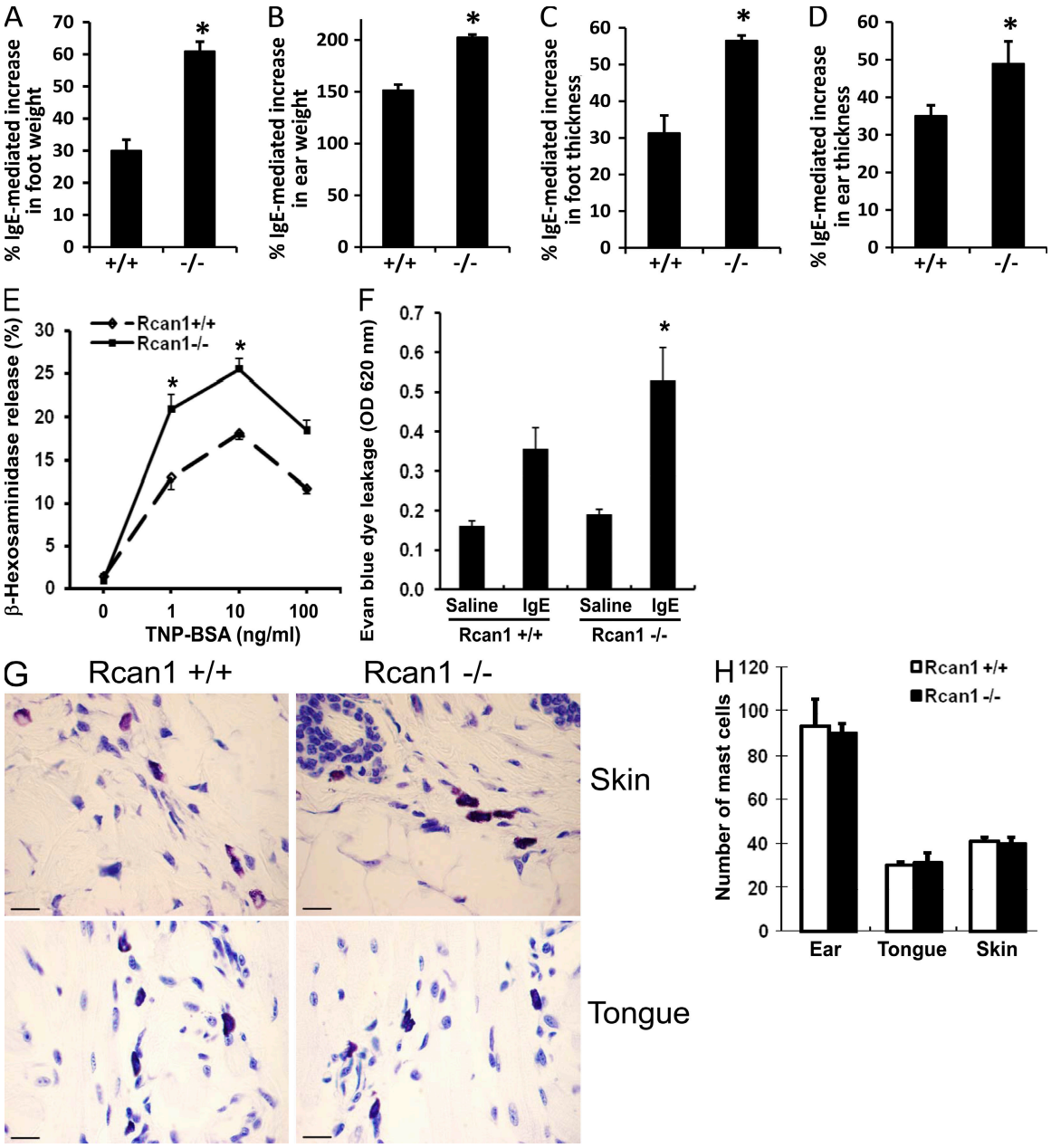

Figure 6. ***Rcan1*** **deficiency leads to enhanced late-phase passive cutaneous anaphylaxis.** (A–D) Mice were passively sensitized by i.v. injection of 2 µg anti-DNP IgE mAb. 24 h later, 20 µl of 0.3% DNFB in acetone/olive oil (4:1) was applied epicutaneously to both sides of the left hind paw or left ear, and 20 µl of acetone/olive oil was applied to the right hind paw or right ear as a control. 24 h later, the thickness of the foot pad and ear was measured using a digital micrometer. The weight of the hind paw and ear punch (5 mm) was also determined. The thickness and weight of the right ear or right hind paw that were treated with acetone/olive oil only were used as baseline values. The DNFB-induced increment of tissue thickness and weight was expressed as a percentage of the baseline values. Data are means ± SEM (n = 10 mice in each group). *, $P < 0.05$ compared with wild-type mice. (E) BMMCs were sensitized with IgE and stimulated with TNP-BSA for 20 min. The release of β-hexosaminidase was determined. Data are means ± SEM (n = 3 independent experiments). *, $P < 0.05$ compared with wild-type BMMCs. (F) Passive cutaneous anaphylaxis. 20 ng anti-DNP IgE was injected intradermally on the left ear, whereas the right ear received saline as a control. After 24 h, mice received 100 µg DNP-BSA containing Evan's blue dye (1% wt/vol) via tail vein injection. Ear punches (8 mm) of both ears were collected 30 min later and were used for extraction of the Evan's blue dye. The optical density was measured at 620 nm. Data are means ± SEM (n = 8 mice in each group). *, $P < 0.05$ compared with the IgE group of the wild-type mice. (G and H) Back skin, tongue, or ear tissues from wild-type or *Rcan1*-deficient mice were fixed and stained by alcian blue for mast cells. Similar metachromatic staining between wild-type and *Rcan1*-deficient mast cells was observed. Specimens were viewed on a microscope (Eclipse E600; Nikon) equipped with a camera (DMX1200; Nikon) and a DDL 20× or 40 ×/0.75 objective lens. Acquisition was performed with Nikon ACT-1 software (version 2.20). Images were processed using Adobe Photoshop software (version 5.0). Slides shown are representative of sections taken from five mice per group. The number of mast cells was enumerated by counting 10 randomly selected fields with a 40 ×/0.75 objective lens (H). Data are means ± SEM (n = 10 fields). Bars, 5 µm.

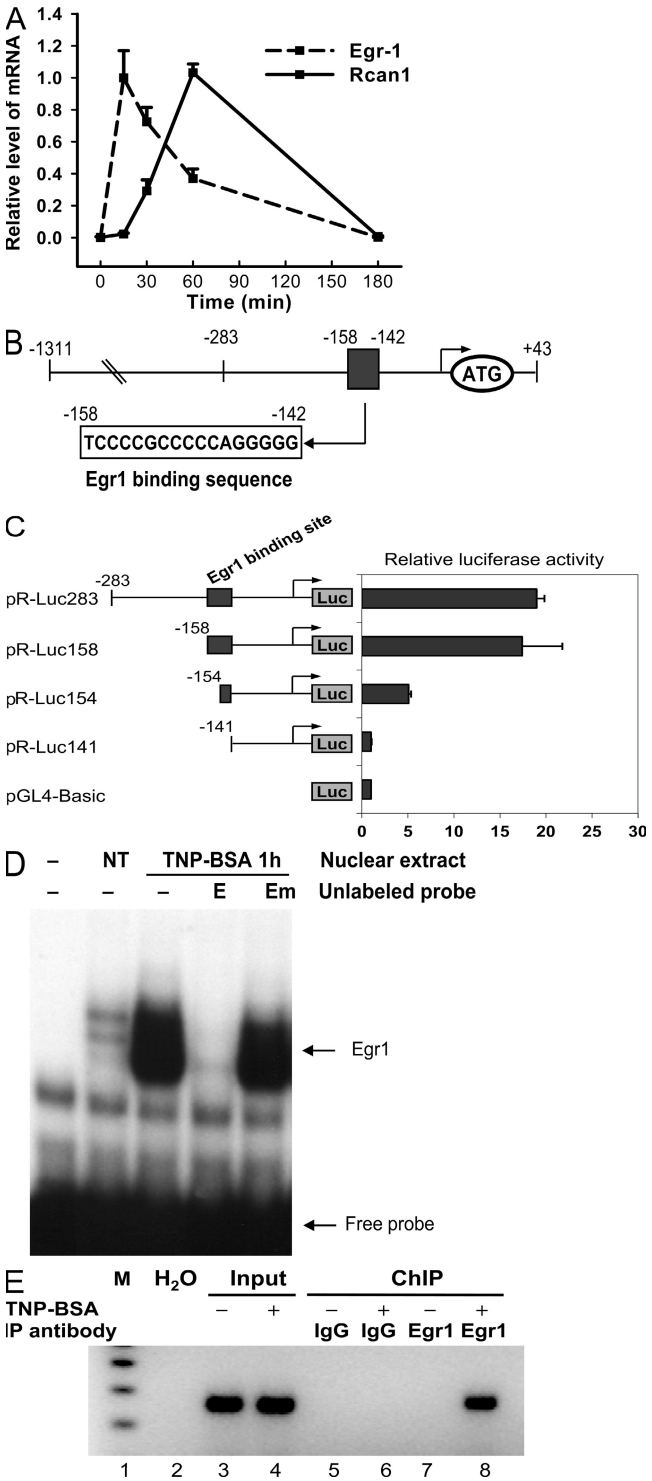

Figure 7. Egr1 binds to and transactivates the *Rcan1* promoter. (A) RNA from TNP-BSA–treated BMMCs was analyzed by real-time quantitative PCR for Egr1 and Rcan1. Egr1 and Rcan1 expression was normalized to endogenous control GAPDH. The data are expressed as relative mRNA levels compared with the mean expression level in BMMCs treated with TNP-BSA for 15 min (=1; Egr1) or for 60 min (=1; Rcan1), because at this time point Egr1 or Rcan1 showed the highest expression level, respectively (n = 3 experiments). (B) The location and sequence of the Egr1 binding site on the *Rcan1* promoter. (C) BMMCs were transfected with various plasmids generated from pGL4 containing different lengths of the Egr1 binding sequence and the control reporter plasmid pRL-TK. All constructs start at −67 bp relative to the ATG codon. The 5′ end of each construct is shown at the left. Firefly and Renilla activities were sequentially quantified using a dual-luciferase reporter assay system. Results are means ± SEM (n = 3). (D) Nuclear proteins from untreated (NT) or TNP-BSA–treated BMMCs (TNP-BSA 1 h) were subjected to EMSA. An Egr1 DNA probe was synthesized based on the Egr1 binding sequences on the *Rcan1* promoter (E). A mutant Egr1 DNA probe with two nucleotide mutations was used for a competition assay (Em). Strong TNP-BSA–induced Egr1 binding was seen and was competed by the specific cold probe (E) but not by the mutant probe (Em). Results are representative of three independent experiments. (E) ChIP assay for the association of Egr1 with *Rcan1* promoter in vivo. BMMCs were stimulated with TNP-BSA for 60 min or left unstimulated. Protein–DNA complexes were extracted and precipitated with anti-Egr1 antibody (Egr1) or control IgG (IgG). DNA from samples before immunoprecipitation (IP) was used as an input control (Input). PCR was performed using primers based on the *Rcan1* promoter sequence. Amplified DNA was resolved in agarose gel. Specific Egr1 binding to the *Rcan1* promoter was seen in TNP-stimulated cells (lane 8) but not in unstimulated cells (lane 7). Results are representative of three independent experiments. M, molecular marker.

decreased luciferase activity. In contrast, the construct pR-luc141, which does not contain an Egr1 binding region, and the empty plasmid pGL4-Basic showed little luciferase activity. This result suggests that the Egr1 binding sequence in the *Rcan1* promoter is functional.

To further confirm that the Egr1 binding sequence is functional in response to FcεRI aggregation, we synthesized a DNA probe containing the Egr1 binding sequence in the *Rcan1* promoter for a gel shift assay. Nuclear proteins were isolated from BMMCs after TNP-BSA stimulation and subjected to EMSA. Strong DNA binding was seen in TNP-BSA–stimulated cells (Fig. 7 D). The binding specificity was confirmed by competition with the nonradiolabeled probe (E, unlabeled probe) but not with a mutant probe (Em, unlabeled probe; Fig. 7 D).

Furthermore, a chromatin immunoprecipitation (ChIP) assay was performed to confirm FcεRI-induced binding of Egr1 to the *Rcan1* promoter. Nuclei from TNP-BSA–stimulated and unstimulated BMMCs were subjected to enzymatic digestion followed by immunoprecipitation using anti-Egr1 or control antibodies. Immunoprecipitates were subjected to PCR using a pair of primers that amplify the *Rcan1* promoter region encompassing the Egr1 binding sequence. Specific Egr1 binding to the *Rcan1* promoter was observed in TNP-BSA–stimulated cells (Fig. 7 E, lane 8) but not in unstimulated cells (Fig. 7 E, lane 7). This result suggested that TNP-BSA stimulation induced Egr1 binding to the *Rcan1* promoter.

Rcan1 expression is diminished in the absence of Egr1

To evaluate whether Egr1 is required for FcεRI-induced Rcan1 expression, we generated *Egr1*-deficient and wild-type BMMCs. *Egr1*-deficient BMMCs mature normally and express similar levels of FcεRI compared with wild-type

BMMCs. BMMCs were sensitized with anti-TNP IgE and stimulated with TNP-BSA. Total RNA was isolated and analyzed by real-time quantitative PCR for Rcan1 (isoform Rcan1-4) expression. TNP-BSA–induced Rcan1 expression was significantly reduced in *Egr1*-deficient BMMCs (Fig. 8 A). A PCR-amplified *Rcan1* product (Rcan1-4) was also separated on an agarose gel. A representative gel is presented in Fig. 8 B. Reduced Rcan1 expression in *Egr1*-deficient BMMCs can be seen after TNP-BSA stimulation. Thus, Egr1 is required for FcεRI-induced Rcan1 expression.

DISCUSSION

The present study demonstrates an as of yet unknown pathway linking activation to inhibition in FcεRI-mediated signaling. Notably, we found that an FcεRI aggregation–induced activation signal initiates de novo synthesis of Rcan1. Rcan1 was identified as a negative regulator, required for turning off FcεRI-activated signals. FcεRI-mediated Rcan1 inhibits calcineurin activity, which leads to down-regulation of NFAT and NF-κB activation, and subsequent cytokine production and inhibition of late-phase allergic reactions. Moreover, Rcan1 is also required for the negative regulation of mast cell degranulation and acute passive cutaneous anaphylaxis. Thus, both the preformed mediator release and the production of newly synthesized cytokines are negatively regulated by Rcan1.

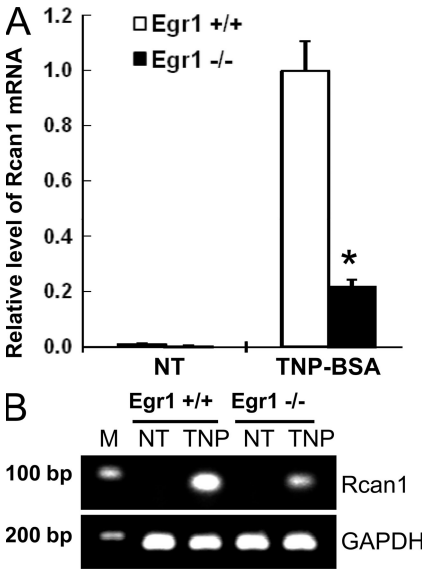

Figure 8. Egr1 is required for Rcan1 expression. (A and B) After sensitization with anti-TNP IgE for 24 h, $Egr1^{+/+}$ and $Egr1^{-/-}$ BMMCs were either not treated (NT) or stimulated with TNP-BSA for 1 h. RNA was isolated and analyzed by real-time quantitative PCR for Rcan1. Rcan1 expression was normalized to endogenous control GAPDH. The data are expressed as relative mRNA levels compared with the mean expression level in $Egr1^{+/+}$ BMMCs treated with TNP-BSA for 60 min (=1), because in this group Rcan1 showed the highest expression level (A). Error bars represent SEs from three independent experiments. *, $P < 0.05$ compared with the wild-type group. The PCR products were also separated by agarose gel and stained with ethidium bromide (B). A representative gel from three independent experiments is shown. M, molecular marker.

It is noteworthy that Rcan1 selectively regulated FcεRI-mediated NFAT and NF-κB pathway but not MAPK and Akt activation. The activity of NFAT is regulated by its phosphorylation state, which is controlled by the opposing action of the serine/threonine phosphatase, calcineurin, and the serine/threonine kinase, glycogen synthase kinase 3 β. Under resting conditions, NFAT is phosphorylated and localized in the cytoplasm. Upon stimulation, it is dephosphorylated by calcineurin and translocates to the nucleus. Studies have indicated that Rcan1 can bind to and inhibit calcineurin (24–26). Thus, it is possible that FcεRI-induced Rcan1 blocks NFAT activation through inhibition of calcineurin. Consistent with this model, we found that calcineurin activity was increased in *Rcan1*-deficient mast cells. Various pharmaceutical molecules targeting the calcineurin–NFAT pathway have successfully been used for the treatment of allergic inflammation (16). This highlights the importance of the NFAT pathway in allergic diseases.

In addition to NFAT activation, we also found that FcεRI-induced IκB phosphorylation and NF-κB activity were enhanced in *Rcan1*-deficient mast cells. Rcan1 is able to regulate the NF-κB pathway through direct interaction with NF-κB–inducing kinase or IκB (27, 28). In addition, calcineurin can dephosphorylate IκB, leading to the subsequent nuclear translocation of NF-κB (15). Thus, Rcan1 could also indirectly regulate the NF-κB pathway through calcineurin. Enhanced FcεRI-induced IκB–NF-κB pathway activation in *Rcan1*-deficient mast cells likely contributes to the increased cytokine production and enhanced late-phase cutaneous allergic reactions.

FcεRI-mediated mast cell production of cytokines such as IL-6, IL-13, and TNF may be beneficial or harmful in the setting of innate or allergic responses. Efficient production of mast cell mediators would be beneficial for the effective development of host defenses, whereas overproduction of mast cell mediators could be harmful. Accordingly, a temporal regulatory mechanism is necessary that allows the initial FcεRI-mediated signaling to proceed in the early phase and permits the termination of the activated signal subsequently in a timely manner. We found that the new synthesis of Rcan1 was dependent on Egr1, which is synthesized de novo after FcεRI stimulation (6). These data suggest that activation signals, including Egr1, proceed to initiate inflammatory cytokine expression, but subsequently Rcan1 is induced, which serves as a negative regulator to inhibit FcεRI-mediated signals by inhibiting calcineurin activity. The new link of Egr1 and Rcan1 may represent a transition from activation to inhibition in FcεRI signaling.

Rcan1 deficiency not only up-regulates cytokine production, it also enhances IgE-dependent mast cell degranulation in vitro and passive cutaneous anaphylaxis in vivo. Calcineurin activity has been associated with mast cell exocytosis (29). Thus, it is possible that Rcan1 modulates IgE-dependent mast cell degranulation and passive cutaneous anaphylaxis through inhibiting calcineurin activity. However, a recent paper demonstrated that Rcan1 regulates vesicle exocytosis

and fusion pore kinetics through novel unknown mechanisms other than calcineurin (30). Indeed, Rcan1 also directly interacts with several additional targets other than calcineurin. These include Raf-1 (31), 14-3-3 (32), and NF-κB–inducing kinase (28). All of these molecules have been directly or indirectly associated with exocytosis.

RCAN1 was first identified as an expressed sequence on a yeast artificial chromosome clone from human chromosome 21 (33). The *Rcan1* gene consists of seven exons, of which exons 1–4 can be alternatively transcribed to produce different mRNA isoforms (17). Members of this new Rcan family also include Rcan2 and Rcan3 (17). The functional distinctions among these family members are unclear. It is interesting to note that the isoform of Rcan1-4, which is encoded by exons 4, 5, 6, and 7, was the only member to be up-regulated by FcεRI aggregation. This result suggests that this isoform may be functionally distinct from the other family members.

Egr1 can be induced by a variety of stimuli such as sepsis (34) and tissue injuries (35). Rcan1 has also been associated with several diseases (36). The link between Egr1 and Rcan1 identified in this study will offer unforeseen potential for the regulation of signaling in a wide range of Egr1- and Rcan1-associated physiological processes and human diseases.

MATERIALS AND METHODS

Animals. *Rcan1*-deficient mice were generated as previously described (18). *Egr1*-deficient mice and control C57BL/6NTac mice were purchased from Taconic. The protocols were approved by the University Committee on Laboratory Animals, Dalhousie University, in accordance with the guidelines of the Canadian Council on Animal Care.

Antibodies. Antibody to Rcan1 (AP6315c) was purchased from Abgent Inc. Antibodies to phospho-JNK (Thr 183/Tyr 185), JNK, phospho-p38 MAPK (Thr 180/Tyr 182), phospho-Syk (Tyr 352), phospho-Akt (Ser 473), and Akt were purchased from Cell Signaling Technology. Antibodies to p38 MAPK and actin were purchased from Santa Cruz Biotechnology, Inc. FITC-conjugated rat anti–mouse CD117 (c-kit) mAb and FITC–rat IgG2a were purchased from Cedarlane Laboratories Ltd. FITC-conjugated rat anti–mouse IgE (IgG1) and FITC–rat IgG1 were purchased from BD.

Mast cell culture and activation. Mouse primary cultured BMMCs were cultured as previously described (6). BMMCs were passively sensitized with IgE from TIB-141 cells (American Type Culture Collection). Cells were then stimulated with 10 ng/ml TNP-BSA (Biosearch Technologies). Mast cell degranulation was determined by measuring β-hexosaminidase release.

Nuclear extract preparation and EMSA. Nuclear protein extracts were obtained using a nuclear extract kit (Active Motif) according to the manufacturer's protocol. EMSA was performed as previously described (6). The following synthesized double-stranded oligonucleotides (Sigma-Aldrich) were used: NFAT binding concensus sequence (N) on mouse IL-13 promoter 5′-AAGGTGTTTCCCCAAGCCTTTCCC-3′ and the mutant sequence (mutant Nm) 5′-AAGGTGT*CCAT*CCAAGCCT*CCTA*C-3′; and Egr1 binding concensus sequence (E) on *Rcan1* promoter 5′-TCCCC-GCCCCCAGGGGGCTGGCTCTCC-3′ and the mutant sequence (Em) 5′-TCCCC*TA*CCCCAGGGGGCTGGCTCTCC-3′ (italics indicate mutated sequences). For competition assays, 1 μl nonradiolabeled wild-type or mutant oligonucleotides (50-fold excess of radiolabeled probe) were added and incubated for 15 min before the addition of the radiolabeled probe. For supershift assay, 4 μg NFATc1 (Thermo Fisher Scientific) or NFATc2 (Santa Cruz Biotechnology, Inc.) was added and incubated for 30 min before the addition of the radiolabeled probe.

Real-time quantitative PCR. The mRNA levels of various genes were quantified using TaqMan MGB probes and TaqMan Master Mix on a sequence detection system (ABI Prism 7000; Applied Biosystems). GAPDH was used as an endogenous reference. Data were analyzed using the relative standard curve method according to the manufacturer's protocol. A mean value of each gene after GAPDH normalization at the time point showing highest expression was used as a calibrator to determine the relative levels of Rcan1, IL-6, TNF, IL-13, IκBα, or Egr1 at different conditions. In addition, PCR products were resolved on a 2% agarose gel and stained with ethidium bromide.

Western blot analysis. Cells lysates (20–30 μg) were subjected to electrophoresis in 12% SDS-polyacrylamide gels. Gels were transferred to polyvinylidene difluoride membrane, blotted with primary and secondary antibodies, and detected by an enhanced chemiluminescence detection system (Western Lightning Plus-ECL; PerkinElmer).

Rcan1 expression vector and transfection. Rcan1 expression vector was constructed by inserting the *Rcan1* gene into pCMV plasmid. BMMCs were resuspended at 4×10^6 cells/transfection in Amaxa nucleofector solution and electroporated with 8 μg DNA using Amaxa Nucleofector Device (program U-023). After 24 h, mast cells were sensitized with IgE for 18 h and challenged with 10 ng/ml TNP-BSA for 6 h.

Calcineurin activity assay. Phosphatase activity was measured using a calcineurin assay kit (BIOMOL International L.P.). Wild-type and *Rcan1*-deficient BMMCs were sensitized with IgE and stimulated with 10 ng/ml TNP-BSA for 6 h. Lysates were prepared, and phosphatase activity was measured according to the manufacturer's instructions.

ChIP. ChIP assays were performed using the ChIP-IT kit (Active Motif) according to the manufacturer's instructions. In brief, BMMCs were fixed with 1% formaldehyde, and the nuclei were subjected to an enzymatic digestion with 5 U of enzymatic shearing cocktail solution for 25 min at 37°C. Sheared chromatin was immunoprecipitated with 4 μg Egr1 (Santa Cruz Biotechnology, Inc.) or control IgG (Active Motif). 0.4% of the input DNA and 5% of the precipitated DNA were then used as templates for each PCR, consisting of 36 cycles of 20 s at 94°C, 30 s at 59°C, and 30 s at 72°C. PCR products were separated by a 2% agarose gel. Primers for amplification of the *Rcan1* promoter region were 5′-AGCAAACCTTAGCGCCTTTT-3′ (forward) and 5′-AAGAGAACGAGCGAGACCAC-3′ (reverse).

Construction of luciferase plasmids. The plasmid pGL4.10 [Luc2] (Promega) was used to construct pR-Luc plasmids containing *Rcan1* promoter fragments. A fragment of the *Rcan1* promoter (−283 to −67, relative to the transcription start site) was generated by PCR with the forward primer 5′-GCTCTAGACTAAGGTGTTGACGTCACC-3′ (*XbaI* site underlined) and the reverse primer 5′-TTTAAGCTTCCTTTGCAAGAGAACGAGCG-3′ (*HindIII* site underlined). The PCR product was purified, digested with *XbaI* and *HindIII*, and ligated into the *NheI*/*HindIII* sites of pGL4.10 using T4 DNA ligase and sequenced to verify orientation. It was designated as pR-Luc283. To generate progressive 5′-unidirectional truncations by PCR, a series of forward primers was used in combination with the same reverse primer and pR-Luc283 as the template. The forward primers began with −158 (5′-CTGGAAGC-CAAGATCTCCCCG-3′; *BglII* site underlined), −154 (5′-GAAGC-CAAGCGGTACCGCCC-3′; *KpnI* site underlined), and −141 (5′-CCAGG CAGCTGGCTCTCCGCG-3′; *PvuII* site underlined). The purified PCR products were digested with corresponding restriction enzymes, treated with mung bean exonuclease, and subcloned into the *EcoRV*/*HindIII* sites of pGL4.10. They were designated pR-Luc158, pR-Luc154, and pR-Luc141, respectively. Each construct was verified by sequencing the insert and plasmid-flanking region.

Luciferase assay. 4×10^6 BMMCs were cotransfected with 3 μg of various luciferase plasmids and 1 μg of control plasmid (pRL-TK; Promega) using a mouse T cell nucleofector kit (Amaxa) and the Amaxa Nucleofector Device (program U-023). Luciferase plasmids used include pNFAT-Luc plasmid (Agilent Technologies), pNF-κB-Luc, and pGL4-Luc containing different *Rcan1* promoter regions. After electroporation, BMMCs were plated in culture medium and allowed to recover for 24 h. Subsequently, the cells were sensitized with anti-TNP IgE for 18 h and challenged with TNP-BSA for 5 or 18 h. Firefly and Renilla activities were sequentially quantified using a dual-luciferase reporter assay system (Agilent Technologies).

Subtractive hybridization. Total RNA (0.6 μg) from no treatment and TNP-treated BMMCs were reverse transcribed using the SMART PCR cDNA Synthesis Kit (Clontech Laboratories, Inc.) and amplified in 19 cycles of PCR, according to the manufacturer's protocol. These cDNAs were subjected to two rounds of subtractive hybridization using the PCR-Select cDNA Subtraction Kit (Clontech Laboratories, Inc.). Forward-subtracted cDNA (no treatment cDNA as driver and TNP-treated adaptor-ligated cDNA as tester) was amplified by two rounds of nested PCR using adaptor-specific primers and Platinum High Fidelity Taq Polymerase (Invitrogen). The resulting PCR products were treated with Taq polymerase (Invitrogen) for 10 min and purified using a MinElute column (QIAGEN) before subcloning into the pCR4-TOPO TA cloning vector (Invitrogen). The ligations were transformed into TOP10 chemically competent cells and plated on lysogeny broth (LB) agar (Invitrogen) containing 100 μg/ml ampicillin (Sigma-Aldrich). Transformed colonies were picked into separate wells of 96-well plates containing 100 μl of LB ampicillin, grown for 4 h, arrayed onto four Hybond-N+ membranes (GE Healthcare), and grown overnight on LB agar supplemented with ampicillin. The colonies were lysed and fixed to the Hybond-N+ membranes using 0.5 M NaOH/1.5 M NaCl, neutralized with 1.5 M NaCl/1 M Tris (pH 7.4), and UV cross-linked in a UV Stratalinker (Agilent Technologies). The forward- and back-subtracted nested PCR products, as well as nonsubtracted tester control and nonsubtracted driver control PCR products, were digested with EagI (New England Biolabs, Inc.) to remove the adaptor sequences, purified with a MinElute column, and labeled with α-[^{32}P]dCTP (GE Healthcare) using the RediPrime labeling kit (GE Healthcare). Unincorporated nucleotide was removed using MicroSpin G-25 columns (GE Healthcare). Each denatured probe (2.5×10^6 dpm) was hybridized with one membrane in 20 ml of Church and Gilbert's buffer overnight at 70°C. The membranes were washed and exposed to Hyperfilm (GE Healthcare). Clones that only hybridized with the forward-subtracted probe were picked into LB AMP, and plasmid DNA was extracted using the Qiaprep Spin Kit (QIAGEN). DNA sequencing was performed on a capillary sequencer (CEQ8000; Beckman Coulter) using the M13rev primer.

Sequence analysis. DNA sequence analysis was performed using the DNAStar Megalign program. Sequence homologies were determined at the National Center for Biotechnology Information using the BLAST program.

IgE-mediated passive cutaneous anaphylaxis. Mice were sensitized by intradermal injection of 20 ng anti-DNP IgE mAb (Sigma-Aldrich) into the left ears, whereas the right ears received saline as a control. After 24 h, mice were challenged by i.v. injection of 100 μg DNP-BSA in 200 μl of Evan's blue dye (1% wt/vol; Sigma-Aldrich). 30 min later, an 8-mm ear punch was collected in 300 μl of formamide and incubated at 80°C for 2 h in water bath to extract the Evan's blue dye. The absorbance was determined at 620 nm.

IgE-mediated late-phase cutaneous reactions. Mice were passively sensitized by i.v. injection of 2 μg anti-DNP IgE mAb (Sigma-Aldrich). After 24 h, a cutaneous reaction was elicited by the application of 20 μl DNFB (0.3% wt/vol; Sigma-Aldrich) in acetone/olive oil (4:1) to both sides of the left hind paw or left ear, and 20 μl of acetone/olive oil to the right hind paw or right ear as a control. The thickness of the foot pad or ear was measured using a digital micrometer after 24 h. The weight of the hind paw or ear punch (5 mm) was also determined. The thickness and weight of the right ear or right hind paw (treated with acetone/olive oil only) were used as baseline values. The DNFB-induced increment of tissue thickness and weight was expressed as a percentage of the baseline values.

Statistical analysis. Analysis of variance and the paired Student's *t* test were used for statistical evaluation of data. Results were considered significant when $P < 0.05$. Throughout the paper, data are expressed as means ± SEM.

Online supplemental materials. Fig. S1 shows the subtraction efficiency of the SSH method using RNAs from TNP-stimulated and unstimulated mast cells. Fig. S2 shows the gene location of the clones identified by SSH. Fig. S3 shows normal maturation of BMMCs from *Rcan1*-deficient mice. Fig. S4 shows increased nuclear translocation of NFAT in *Rcan1*-deficient mast cells compared with wild-type mast cells after TNP-BSA stimulation. Fig. S5 shows increased IκBα synthesis (particularly at 60 min) in *Rcan1*-deficient mast cells after TNP-BSA stimulation. Table S1 shows eight Rcan1 clones and one Egr1 clone identified by SSH. Online supplemental material is available at http://www.jem.org/cgi/content/full/jem.20081140/DC1.

We thank F. Liu for her assistance in cell culture and passive cutaneous anaphylaxis assays.

T.-J. Lin is supported by grants from the Canadian Institutes of Health Research (MOP 68815 and MOP 81355), the Canadian Cystic Fibrosis Foundation, and the Izaak Walton Killam (IWK) Health Center. J. Molkentin is supported by a grant from the National Institutes of Health. J. Berman is supported by grants from the Canadian Institutes of Health Research (ROP 85505), the Nova Scotia Health Research Foundation, and the IWK Health Center. Y.J. Yang is supported by a postdoctoral fellowship from the IWK Health Center.

The authors have no conflicting financial interests.

Submitted: 27 May 2008
Accepted: 4 December 2008

REFERENCES

1. Kawakami, T., and S.J. Galli. 2002. Regulation of mast-cell and basophil function and survival by IgE. *Nat. Rev. Immunol.* 2:773–786.
2. Molfetta, R., G. Peruzzi, A. Santoni, and R. Paolini. 2007. Negative signals from FcepsilonRI engagement attenuate mast cell functions. *Arch. Immunol. Ther. Exp. (Warsz.).* 55:219–229.
3. Kinet, J.P. 1999. The high-affinity IgE receptor (Fc epsilon RI): from physiology to pathology. *Annu. Rev. Immunol.* 17:931–972.
4. Eiseman, E., and J.B. Bolen. 1992. Engagement of the high-affinity IgE receptor activates src protein-related tyrosine kinases. *Nature.* 355: 78–80.
5. Parravicini, V., M. Gadina, M. Kovarova, S. Odom, C. Gonzalez-Espinosa, Y. Furumoto, S. Saitoh, L.E. Samelson, J.J. O'Shea, and J. Rivera. 2002. Fyn kinase initiates complementary signals required for IgE-dependent mast cell degranulation. *Nat. Immunol.* 3:741–748.
6. Li, B., M.R. Power, and T.J. Lin. 2006. De novo synthesis of early growth response factor-1 is required for the full responsiveness of mast cells to produce TNF and IL-13 by IgE and antigen stimulation. *Blood.* 107: 2814–2820.
7. Kramer, B., A. Meichle, G. Hensel, P. Charnay, and M. Kronke. 1994. Characterization of an Krox-24/Egr-1-responsive element in the human tumor necrosis factor promoter. *Biochim. Biophys. Acta.* 1219:413–421.
8. Decker, E.L., N. Nehmann, E. Kampen, H. Eibel, P.F. Zipfel, and C. Skerka. 2003. Early growth response proteins (EGR) and nuclear factors of activated T cells (NFAT) form heterodimers and regulate proinflammatory cytokine gene expression. *Nucleic Acids Res.* 31:911–921.
9. Faour, W.H., N. Alaaeddine, A. Mancini, Q.W. He, D. Jovanovic, and J.A. Di Battista. 2005. Early growth response factor-1 mediates prostaglandin E2-dependent transcriptional suppression of cytokine-induced tumor necrosis factor-alpha gene expression in human macrophages and rheumatoid arthritis-affected synovial fibroblasts. *J. Biol. Chem.* 280:9536–9546.
10. Thottassery, J.V., D. Sun, G.P. Zambetti, A. Troutman, V.P. Sukhatme, E.G. Schuetz, and J.D. Schuetz. 1999. Sp1 and egr-1 have opposing

effects on the regulation of the rat Pgp2/mdr1b gene. *J. Biol. Chem.* 274:3199–3206.
11. Nguyen, H.Q., B. Hoffman-Liebermann, and D.A. Liebermann. 1993. The zinc finger transcription factor Egr-1 is essential for and restricts differentiation along the macrophage lineage. *Cell.* 72:197–209.
12. Hutchinson, L.E., and M.A. McCloskey. 1995. Fc epsilon RI-mediated induction of nuclear factor of activated T-cells. *J. Biol. Chem.* 270: 16333–16338.
13. Marquardt, D.L., and L.L. Walker. 2000. Dependence of mast cell IgE-mediated cytokine production on nuclear factor-kappaB activity. *J. Allergy Clin. Immunol.* 105:500–505.
14. Macian, F. 2005. NFAT proteins: key regulators of T-cell development and function. *Nat. Rev. Immunol.* 5:472–484.
15. Frantz, B., E.C. Nordby, G. Bren, N. Steffan, C.V. Paya, R.L. Kincaid, M.J. Tocci, S.J. O'Keefe, and E.A. O'Neill. 1994. Calcineurin acts in synergy with PMA to inactivate I kappa B/MAD3, an inhibitor of NF-kappa B. *EMBO J.* 13:861–870.
16. Carroll, C.L., and A.B. Fleischer Jr. 2006. Tacrolimus: focusing on atopic dermatitis. *Drugs Today (Barc).* 42:431–439.
17. Davies, K.J., G. Ermak, B.A. Rothermel, M. Pritchard, J. Heitman, J. Ahnn, F. Henrique-Silva, D. Crawford, S. Canaider, P. Strippoli, et al. 2007. Renaming the DSCR1/Adapt78 gene family as RCAN: regulators of calcineurin. *FASEB J.* 21:3023–3028.
18. Sanna, B., E.B. Brandt, R.A. Kaiser, P. Pfluger, S.A. Witt, T.R. Kimball, E. van Rooij, L.J. De Windt, M.E. Rothenberg, M.H. Tschop, et al. 2006. Modulatory calcineurin-interacting proteins 1 and 2 function as calcineurin facilitators in vivo. *Proc. Natl. Acad. Sci. USA.* 103: 7327–7332.
19. Li, Q., and I.M. Verma. 2002. NF-kappaB regulation in the immune system. *Nat. Rev. Immunol.* 2:725–734.
20. Peng, Y., M.R. Power, B. Li, and T.J. Lin. 2005. Inhibition of IKK down-regulates antigen + IgE-induced TNF production by mast cells: a role for the IKK-IkappaB-NF-kappaB pathway in IgE-dependent mast cell activation. *J. Leukoc. Biol.* 77:975–983.
21. Kawakami, Y., S.E. Hartman, P.M. Holland, J.A. Cooper, and T. Kawakami. 1998. Multiple signaling pathways for the activation of JNK in mast cells: involvement of Bruton's tyrosine kinase, protein kinase C, and JNK kinases, SEK1 and MKK7. *J. Immunol.* 161:1795–1802.
22. Wershil, B.K., Z.S. Wang, J.R. Gordon, and S.J. Galli. 1991. Recruitment of neutrophils during IgE-dependent cutaneous late phase reactions in the mouse is mast cell-dependent. Partial inhibition of the reaction with antiserum against tumor necrosis factor-alpha. *J. Clin. Invest.* 87:446–453.
23. Nagai, H., T. Abe, I. Yamaguchi, K. Mito, M. Tsunematsu, M. Kimata, and N. Inagaki. 2000. Role of mast cells in the onset of IgE-mediated late-phase cutaneous response in mice. *J. Allergy Clin. Immunol.* 106:S91–S98.
24. Rothermel, B., R.B. Vega, J. Yang, H. Wu, R. Bassel-Duby, and R.S. Williams. 2000. A protein encoded within the Down syndrome critical region is enriched in striated muscles and inhibits calcineurin signaling. *J. Biol. Chem.* 275:8719–8725.
25. Rothermel, B.A., R.B. Vega, and R.S. Williams. 2003. The role of modulatory calcineurin-interacting proteins in calcineurin signaling. *Trends Cardiovasc. Med.* 13:15–21.
26. Fuentes, J.J., L. Genesca, T.J. Kingsbury, K.W. Cunningham, M. Perez-Riba, X. Estivill, and S. de la Luna. 2000. DSCR1, overexpressed in Down syndrome, is an inhibitor of calcineurin-mediated signaling pathways. *Hum. Mol. Genet.* 9:1681–1690.
27. Kim, Y.S., K.O. Cho, H.J. Lee, S.Y. Kim, Y. Sato, and Y.J. Cho. 2006. Down syndrome candidate region 1 increases the stability of the IkappaBalpha protein: implications for its anti-inflammatory effects. *J. Biol. Chem.* 281:39051–39061.
28. Lee, E.J., S.R. Seo, J.W. Um, J. Park, Y. Oh, and K.C. Chung. 2008. NF-kappaB-inducing kinase phosphorylates and blocks the degradation of Down syndrome candidate region 1. *J. Biol. Chem.* 283: 3392–3400.
29. Hultsch, T., P. Brand, S. Lohmann, J. Saloga, R.L. Kincaid, and J. Knop. 1998. Direct evidence that FK506 inhibition of FcepsilonRI-mediated exocytosis from RBL mast cells involves calcineurin. *Arch. Dermatol. Res.* 290:258–263.
30. Keating, D.J., D. Dubach, M.P. Zanin, Y. Yu, K. Martin, Y.F. Zhao, C. Chen, S. Porta, M.L. Arbones, L. Mittaz, and M.A. Pritchard. 2008. DSCR1/RCAN1 regulates vesicle exocytosis and fusion pore kinetics: implications for Down syndrome and Alzheimer's disease. *Hum. Mol. Genet.* 17:1020–1030.
31. Cho, Y.J., M. Abe, S.Y. Kim, and Y. Sato. 2005. Raf-1 is a binding partner of DSCR1. *Arch. Biochem. Biophys.* 439:121–128.
32. Abbasi, S., J.D. Lee, B. Su, X. Chen, J.L. Alcon, J. Yang, R.E. Kellems, and Y. Xia. 2006. Protein kinase-mediated regulation of calcineurin through the phosphorylation of modulatory calcineurin-interacting protein 1. *J. Biol. Chem.* 281:7717–7726.
33. Fuentes, J.J., M.A. Pritchard, A.M. Planas, A. Bosch, I. Ferrer, and X. Estivill. 1995. A new human gene from the Down syndrome critical region encodes a proline-rich protein highly expressed in fetal brain and heart. *Hum. Mol. Genet.* 4:1935–1944.
34. Pawlinski, R., B. Pedersen, B. Kehrle, W.C. Aird, R.D. Frank, M. Guha, and N. Mackman. 2003. Regulation of tissue factor and inflammatory mediators by Egr-1 in a mouse endotoxemia model. *Blood.* 101: 3940–3947.
35. Yan, S.F., T. Fujita, J. Lu, K. Okada, Y. Shan Zou, N. Mackman, D.J. Pinsky, and D.M. Stern. 2000. Egr-1, a master switch coordinating upregulation of divergent gene families underlying ischemic stress. *Nat. Med.* 6:1355–1361.
36. Harris, C.D., G. Ermak, and K.J. Davies. 2005. Multiple roles of the DSCR1 (Adapt78 or RCAN1) gene and its protein product calcipressin 1 (or RCAN1) in disease. *Cell. Mol. Life Sci.* 62:2477–2486.